Characterizations of Cobalt Oxide Nanoparticles within Faujasite Zeolites and the Formation of Metallic Cobalt

Qinghu Tang, Qinghong Zhang, Ping Wang, Ye Wang,* and Huilin Wan

State Key Laboratory of Physical Chemistry of Solid Surfaces, Department of Chemistry, Xiamen University, Xiamen 361005, China

Received October 6, 2003. Revised Manuscript Received March 3, 2004

Cobalt oxide (CoO_x) particles within faujasite zeolites have been synthesized by a procedure comprising (i) ion-exchange of cobalt ions into the zeolite, (ii) precipitation of cobalt ions with sodium hydroxide within the supercages of the zeolite, and (iii) calcination. The materials are characterized by XRD, nitrogen sorption, XPS, TEM-EDS, H_2-TPR, and O_2-titration. The concentration of sodium hydroxide for precipitation and the temperature for calcination are found to be critical in controlling the locations of the CoO_x particles. With appropriate conditions, the CoO_x particles formed are located and encapsulated in the supercages of faujasite zeolites. The sizes of the CoO_x particles are in the range of 0.7−3 nm with a maximum distribution of 1.3−1.5 nm. These particles exist mainly in the state of CoO. On the other hand, higher calcination temperature or higher concentration of sodium hydroxide may lead to the formation of larger Co_3O_4 particles located outside the supercages of the faujasite zeolites. The CoO_x particles encapsulated in the supercages exhibit a broad reduction peak and can be partly reduced to metallic cobalt at temperatures as low as 573 K, while the cobalt cations exchanged into the zeolites can only be reduced at temperatures higher than 773 K. The metallic cobalt formed by the reduction of cobalt oxide within the supercage exhibits superior catalytic activity in Fischer−Tropsch synthesis.

Introduction

Metal and metal oxide nanoparticles have attracted increased attention due to their unusual physical and chemical properties. Many methods have been developed for the synthesis of nanoparticles.[1] Among them, the utilization of microporous and mesoporous materials as the hosts for generating metal and metal oxide nanoparticles represents an especially promising direction.[2−22] Faujasite zeolites, including X- and Y-type zeolite, possess supercages with a diameter of ca. 1.3 nm in their structures and may be used for the assembly of metal or metal oxide nanoparticles of sizes less than 2 nm, because the pore size restriction could limit the growth of the particles.

Thus far, the preparation of nanoparticles or clusters of noble metals such as Pd, Pt, and Rh within faujasite zeolites have been intensively studied.[2−6] A typical and convenient procedure for generating nanoparticles of noble metals inside zeolite pores is to introduce metal cations into the zeolite by ion-exchange and then to treat the ion-exchanged material with a reductant such as H_2 or CO.[2,3,6] When this procedure is applied to the synthesis of nonnoble transition metals such as Fe and

* To whom correspondence should be addressed. Tel: (+86) 592−2187470. Fax: (+86) 592-2183047. E-mail: yewang@jingxian.xmu.edu.cn.

(1) (a) Schmid, G.; Bäumle, M.; Geerkens, M.; Heim, I.; Osemann, C.; Sawitowski, T. *Chem. Soc. Rev.* **1999**, *28*, 179. (b) Rao, C. N. R.; Kulkarni, G. U.; Thomas, P. J.; Edwards, P. P. *Chem. Soc. Rev.* **2000**, *29*, 27. (c) Trindade, T.; O'Prien, P.; Pickett, N. L. *Chem. Mater.* **2001**, *13*, 3843.

(2) (a) Tzou, M. S.; Teo, B. K.; Sachtler, W. M. H. *J. Catal.* **1988**, *113*, 220. (b) Homeyer, S. T.; Sachtler, W. M. H. *J. Catal.* **1989**, *117*, 91. (c) Homeyer, S. T.; Sachtler, W. M. H. *J. Catal.* **1989**, *118*, 266. (d) Feeley, J. S.; Sachtler, W. M. H.; *J. Catal.* **1991**, *131*, 573. (e) Zhang, Z.; Zhang, Y. D.; Hines, W. A.; Budnick, J. I.; Sachtler, W. M. H. *J. Am. Chem. Soc.* **1992**, *114*, 4834.

(3) de Mallmann, A.; Barthomeuf, D. *J. Chim. Phys.-Chim. Biol.* **1990**, *87*, 535.

(4) Ryoo, R.; Cho, S. J.; Pak, C. H.; Kim, J. G.; Ihm, S. K.; Lee, J. Y. *J. Am. Chem. Soc.* **1992**, *114*, 76.

(5) Kawi, S.; Chang, J. R.; Gates, B. C. *J. Am. Chem. Soc.* **1993**, *115*, 4830.

(6) de Graaf, J.; van Dillen, A. J.; de Jong, K. P.; Koningsberger, D. C. *J. Catal.* **2001**, *203*, 307.

(7) Guczi, L.; Beck, A.; Horváth, A.; Horváth, D. *Top. Catal.* **2002**, *19*, 2.

(8) Wark, M.; Kessler, H.; Schulz-Ekloff, G. *Microporous Mater.* **1997**, *8*, 241.

(9) Mulukutla, R. S.; Asakura, K.; Namba, S.; Iwasawa, Y. *Chem. Commun.* **1998**, 1425.

(10) Seidel, A.; Loos, J.; Boddenberg, B. *J. Mater. Chem.* **1999**, *9*, 2495.

(11) Zhang, W.; Shi, J.; Wang, L.; Yang, D. *Chem. Mater.* **2000**, *12*, 1408.

(12) Grubert, G.; Stockenhuber, M.; Tkachenko, O. P.; Wark, M. *Chem. Mater.* **2002**, *14*, 2458.

(13) Zhang, L. X.; Shi, J. L.; Yu, J.; Hua, Z. L.; Zhao, X. G.; Ruan, M. L. *Adv. Mater.* **2002**, *14*, 1510.

(14) Gies, H.; Grabowski, S.; Bandyopadhyay, M.; Grünert, W.; Tkachenko, O. P.; Klementiev, K. V.; Birkner, A. *Microporous Mesoporous Mater.* **2003**, *60*, 31.

(15) Huwe, H.; Fröba, M. *Microporous Mesoporous Mater.* **2003**, *60*, 151.

(16) Yang, C.; Liu, P.; Ho, Y.; Chiu, C.; Chao, K. *Chem. Mater.* **2003**, *15*, 275.

(17) Kónya, Z.; Puntes, V. F.; Kiricsi, I.; Zhu, J.; Ager, J. W.; Ko, M. K.; Frei, H.; Alivisatos, P.; Somorjai, G. A. *Chem. Mater.* **2003**, *15*, 1242.

(18) Dong, A.; Wang, Y.; Tang, Y.; Ren, N.; Zhang, Y.; Gao, Z. *Chem. Mater.* **2003**, *14*, 3217.

(19) Wakayama, H.; Setoyama, N.; Fukushima, Y. *Adv. Mater.* **2003**, *15*, 742.

(20) Zhan, B.-Z.; White, M. A.; Sham, T.-K.; Pincock, J. A.; Doucet, R. J.; Rao, R.; Robertson, K. N.; Cameron, T. S. *J. Am. Chem. Soc.* **2003**, *125*, 2195.

(21) Fröba, M.; Köhn, R.; Bouffaud, G.; Richard, O.; van Tendeloo, G. *Chem. Mater.* **1999**, *11*, 2858.

(22) Köhn, R.; Fröba, M. *Catal. Today* **2001**, *68*, 227.

10.1021/cm030626z CCC: $27.50
Published on Web 04/09/2004

Co, which are also very important in catalysis or other fields, the reduction of metal cationic precursors inside the cages or pores of zeolite becomes difficult at moderate temperatures of less than 800 K.[23] Higher reduction temperatures, however, may lead to the migration of a large proportion of metals out of the zeolite pores or the destruction of the zeolite framework. The difficulty in the reduction of the nonnoble metal cations is believed to arise from the strong interaction between the cationic precursor and the anionic zeolite framework.

Only very scattered studies have contributed to the synthesis of nonnoble transition metals encapsulated within zeolite cages. The treating of transition-metal-exchanged zeolites with sodium hydroxide[24,25] or sodium acetate[26] has been reported to enhance the reduction of cobalt precursors at relatively low temperatures. However, the details about the changes in the cobalt precursors after the treatment and the roles of sodium acetate or sodium hydroxide are not unambiguous in those studies. On the other hand, Wark and co-workers have addressed the formation of zinc or cadmium oxide with sizes of 1−10 nm inside zeolite Y by a method starting with ion-exchange to introduce Zn^{2+} or Cd^{2+} into zeolites followed by the treatment with sodium hydroxide solution and subsequent calcination.[8] It is reasonable to consider that this method may likewise be applied to the synthesis of other metal oxides within zeolites and this may lead to an efficient way to assemble nonnoble transition-metal nanoparticles inside the pores of zeolites, since it can be expected that the reduction of such formed metal oxides may become easier as compared with the corresponding metal cations.

The elucidation of the nature and the locations of metal oxides prepared by this method and the clarification of the critical factors controlling the states of these metal oxides are thus of great significance. Recently, we have focused on the investigation of cobalt oxide introduced into faujasite zeolites by this method and its subsequent reduction to metallic cobalt with H_2. It is known that cobalt is an effective catalytic component in Fischer−Tropsch synthesis, which is an important route for the transformation of natural gas into useful hydrocarbon fuels via synthesis gas.[27] We have recently communicated that cobalt loaded in NaY zeolite exhibits higher activity and selectivity to n-C_{10}−C_{20} paraffins (diesel fuel fraction).[28]

In the present paper, we report detailed characterizations of the cobalt oxide formed within faujasite zeolites by precipitating the Co^{2+}-exchange zeolites with sodium hydroxide solution, followed by calcination. The influences of the concentration of sodium hydroxide and the calcination temperature on the locations and the states of cobalt oxide particles were investigated. The reducibility of the cobalt oxide particles within the zeolites and the catalytic properties of the thus formed metallic cobalt in Fischer−Tropsch synthesis were also studied.

Table 1. Cobalt Content in Samples[a]

sample[b]	concn of $Co(NO_3)_2$ soln used in ion exchange (M)	proportion of Co incorp (%)	degree of exchange (%)	Co content (wt %)
CoO_x-X-2.6	0.01	87	19	2.6
CoO_x-X-5.7	0.02	97	42	5.7
CoO_x-X-8.8	0.1	30	65	8.8
CoO_x-X-8.6	0.2	15	64	8.6
CoO_x-X-9.5	0.1[c]	11	70	9.5
CoO_x-Y-1.1	0.011[d]	88	13	1.1
CoO_x-Y-2.5	0.022[d]	97	29	2.5
CoO_x-Y-3.5	0.045[d]	67	41	3.5
CoO_x-Y-6.2	0.1	21	71	6.2

[a] Typical conditions for ion exchange: Na-zeolite, 2.0 g; volume of $Co(NO_3)_2$ aqueous solution, 100 mL. [b] The number after X or Y denotes the cobalt content in weight percentage. [c] The ion exchange was carried out three times. [d] The volume of $Co(NO_3)_2$ aqueous solution for exchange was 40 mL.

Experimental Section

Materials Preparation. Parent faujasite zeolites including NaX with a Si/Al ratio of 1.3 and NaY with a Si/Al ratio of 2.8 were prepared via hydrothermal synthesis using $NaSiO_3 \cdot 9H_2O$, $NaAlO_2$, NaOH, and H_2O as starting materials. The molar composition of the synthesis mixture of Na_2O:Al_2O_3:SiO_2:H_2O was 4.8:1:3.7:180 for the synthesis of NaX and 8:1:10:160 for the synthesis of NaY.

Zeolite-encapsulated cobalt oxide samples (CoO_x-X and CoO_x-Y) were synthesized by the following procedures. In the first step, cobalt cations were introduced into the faujasite zeolite by ion-exchange at room temperature in an aqueous solution of cobalt nitrate for 24 h. The concentration of the aqueous solution was regulated to control the degree of ion-exchange and the cobalt content in the sample (see Table 1 for details). After filtration, washing thoroughly with deionized water, and drying at 393 K, the cobalt ion-containing zeolite was treated with aqueous NaOH solution at room temperature. The concentration of NaOH used under the standard conditions was 0.1 M and was changed from 0.01 to 5 M as the effect of NaOH concentration was investigated. The color of the sample changed from light blue to dark blue during the treatment with NaOH, indicating that the precipitation of cobalt hydroxide occurred within the zeolite. After treatment for 20 min, the sample was recovered by filtration, followed by washing thoroughly until the pH value of the filtrate decreased to ca. 7 and by drying at 393 K. The resultant powder was finally calcined to obtain the CoO_x-X or CoO_x-Y composites. The calcination temperature was 673 K under the standard conditions and was varied from 573 to 923 K in investigating the effect of the calcination temperature.

Characterization. The content of cobalt in each sample was determined by atomic absorption spectroscopy analysis on a WFX-1C spectrometer after the sample was completely dissolved with diluted nitric acid and a small amount of hydrofluoric acid.

Powder X-ray diffraction (XRD) patterns were recorded with a Rigaku D/Max-C X-ray diffractometer equipped with a rotating anode using Cu Kα radiation (40 kV, 40 mA).

The properties of the porous structures were determined from N_2-sorption measurements at 77 K using a Micromeritics ASAP 2010 system. The sample was outgassed under vacuum at 573 K for 3 h before the adsorption of nitrogen. Pore size distributions in the microporous region (0.5−1.5 nm) were evaluated from the adsorption isotherms by the Horváth−Kawazoe (HK) method,[29] and those in the mesoporous region (2−50 nm) were derived by the BJH method.[30] The mi-

(23) Guczi, L. *Catal. Lett.* **1991**, *7*, 205.
(24) (a) Suzuki, M.; Tsutsumi, K.; Takahashi, H.; Saito, Y. *Zeolite* **1988**, *8*, 284. (b) Suzuki, M.; Tsutsumi, K.; Takahashi, H.; Saito, Y. *Zeolite* **1988**, *8*, 381.
(25) (a) Koh, D. J.; Chung, J. S.; Kim, Y. G. *J. Chem. Soc. Chem. Commun.* **1991**, 849. (b) Chung, J. S.; Yun, H. G.; Koh, D. J.; Kim, Y. G. *J. Mol. Catal.* **1993**, *79*, 199.
(26) Zhang, Z.; Yin, Y.; Sachtler, W. M. H. *Catal. Lett.* **1993**, *18*, 73.
(27) Schulz, H. *Appl. Catal. A* **1999**, *186*, 3.
(28) Tang, Q.; Wang, Y.; Zhang, Q.; Wan, H. *Catal. Commun.* **2003**, *4*, 253.
(29) Horváth, G.; Kawazoe, K. *J. Chem. Eng. Jpn.* **1983**, *16*, 470.
(30) Barrett, E. P.; Joyner, L. S.; Halenda, P. P. *J. Am. Chem. Soc.* **1951**, *73*, 373.

croporous volume was evaluated by the *t*-plot method.[31]

The transmission electron microscopy (TEM) with X-ray energy-dispersive spectroscopic analysis (EDS) was carried out in a FEI Tecnai 30 electron microscope (Phillips Analytical) operated at an acceleration voltage of 300 kV. EDS spectra were generally recorded from the sample with an area of 6 nm in diameter. Samples for TEM measurements were suspended in ethanol and ultrasonically dispersed. Drops of the suspensions were applied on a copper grid coated with carbon.

The X-ray photoelectron spectroscopy (XPS) was measured with a PHI Quantum 2000 Scanning ESCA Microprobe equipment (Physical Electronics) using monochromatic Al Kα radiation ($h\nu = 1846.6$ eV, 25 W). The background pressure in the analysis chamber was lower than 1×10^{-7} Pa. The X-ray beam diameter was 100 μm, and the pass energy was 29.35 eV for each analysis. The binding energy was calibrated using a C 1s photoelectron peak at 284.6 eV as a reference.

The reduction behaviors of the CoO_x-X and CoO_x-Y samples were studied by temperature-programmed reduction with H_2 (H_2-TPR). The H_2-TPR was performed using a flow system equipped with a thermal conductivity detector (TCD). Typically, 100 mg of sample was first pretreated in a quartz reactor with a gas flow containing O_2 and N_2 at 573−923 K (determined by the calcination temperature used for preparation as described above) for 1 h followed by a purge with pure N_2. After cooling to ca. 300 K, a H_2−Ar (5% H_2) mixture was introduced into the reactor and the temperature was raised to 1200 K at a rate of 10 K min^{-1}.

To make quantitative calculations for the degree of reduction, some of the samples, which had been reduced by H_2 at 673 K followed by purging with flowing He at 723 K, were subjected to O_2-titration by introducing O_2 pulses with a volume of 0.1 cm^3 at 723 K. The consumption of O_2 by the reduced catalysts was measured by a TCD.

Measurement of Catalytic Properties. The catalytic properties of the reduced samples in Fischer−Tropsch synthesis were studied. The catalytic reactions were carried out using a fixed-bed flow reactor operated at 2.0 MPa. The CoO_x-X and CoO_x-Y samples loaded in the reactor were first reduced in pure H_2 gas flow (101.3 kPa, 30 mL min^{-1}) at 673 K for 12 h. A H_2 and CO mixture with a H_2/CO ratio of 2 was then introduced into the reactor and the pressure was raised to 2.0 MPa after the temperature was decreased to 523 K. Argon with a concentration of 4% contained in the synthesis gas was used as an internal standard for the calculation of CO conversion. The products with carbon numbers lower than 5 were analyzed by on-line gas chromatography, and those with larger carbon numbers (C_6−C_{25}) were collected by a cold trap during the reaction for 10 h and were analyzed by a gas chromatograph equipped with a capillary column and FID detector. The product distributions of Fischer−Tropsch synthesis generally followed the Anderson−Schulz−Flory distributions, which could be expressed using the equation $M_n = (1 - \alpha)\alpha^{n-1}$, where M_n, n, and α are the molar fraction of each hydrocarbon product, the carbon number, and the chain growth probability, respectively.[32] The chain growth probability, α, was evaluated from the slope of the curve of ln M_n versus n.

Results and Discussion

Degree of Exchange and Cobalt Content. It can be expected that the cobalt content in the material is only determined in the ion-exchange step. The successive steps, i.e., precipitation and calcination, could not influence the total cobalt content in the final materials. Therefore, the numbers of cobalt ions in aqueous solution for ion-exchange and the numbers of exchangeable sites (Na^+) in zeolites as well as the efficiency for ion-exchange would affect the degree of exchange and thus the cobalt content. Under a fixed amount of zeolite and a fixed volume of solution used for ion-exchange, we found that the degree of exchange and thus the cobalt content could be regulated by changing the concentration of the Co^{2+} solution. Table 1 shows the content of cobalt incorporated in each sample synthesized in this work. For both NaX and NaY zeolites, at very low concentrations of Co^{2+}, i.e., a lower amount of Co^{2+} in the solution as compared with the exchangeable sites, almost all the cobalt ions could be incorporated into the zeolite. An increase in the concentration of Co^{2+} resulted in an increase in the degree of exchange and the cobalt content in the final sample, but the proportion of cobalt ions capable of being incorporated into zeolite decreased sharply. A degree of exchange of ca. 65% was obtained in the case of NaX zeolite with a 0.1 M solution of Co-$(NO_3)_2$. A further increase in the concentration did not exert a significant influence on the degree of exchange. Repeating the ion-exchange three times only slightly increased the degree of exchange and the cobalt content.

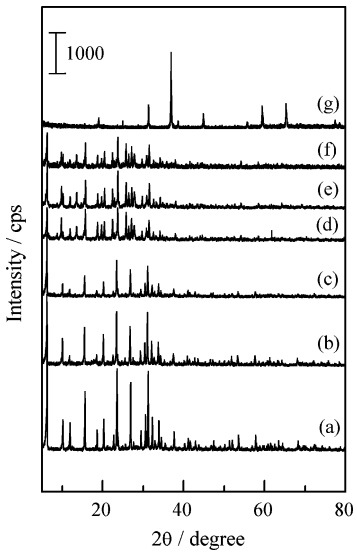

Figure 1. XRD patterns of a series of CoO_x-X and CoO_x-Y samples prepared under the standard conditions, as well as Co_3O_4: (a) NaX, (b) CoO_x-X-8.8-673 K, (c) CoO_x-X-9.5−673 K, (d) NaY, (e) CoO_x-Y-3.5-673 K, (f) CoO_x-Y-6.2-673 K, and (g) Co_3O_4.

XRD Results. Figure 1 shows the XRD patterns of a series of CoO_x-X and CoO_x-Y samples with different cobalt content prepared under the standard conditions (NaOH, 0.1 M; calcination temperature, 673 K) as well as Co_3O_4, the most stable cobalt oxide. Only diffraction peaks ascribed to NaX or NaY were observed for all the CoO_x-X or CoO_x-Y samples prepared here, and peaks of crystalline Co_3O_4 did not appear even for the sample with cobalt content of 9.5 wt % in the case of CoO_x-X or 6.2 wt % in the case of CoO_x-Y. This result suggests that there are no large crystalline Co_3O_4 particles existing in the materials prepared under the standard conditions.

The effects of the preparation conditions on the XRD patterns of the CoO_x-X samples with the same cobalt content (8.8 wt %) were investigated. Figure 2 shows the results obtained by changing the concentration of NaOH in the precipitation step and the calcination temperature. As the concentration of NaOH used for precipitation reached 5.0 M, a weak peak at 36.8°, which

(31) Cranston, R.; Inkley, F. *Adv. Catal.* **1957**, *9*, 143.
(32) van der Lann, G. P.; Beenackers, A. A. C. M. *Catal. Rev. Sci. Eng.* **1999**, *41*, 255.

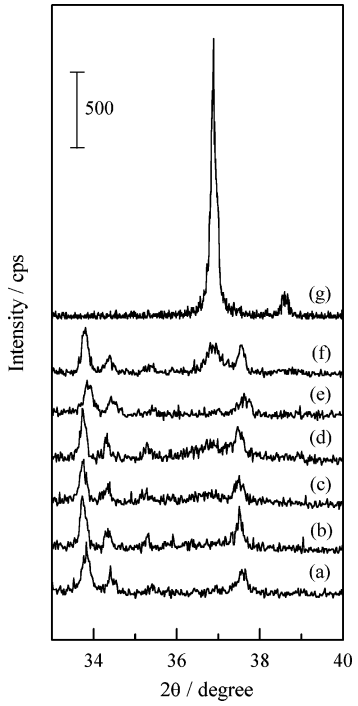

Figure 2. XRD patterns of the CoO_x-X samples with the cobalt content of 8.8 wt % prepared under different conditions as well as Co_3O_4: (a) CoO_x-X-8.8-0.1 M-673 K, (b) CoO_x-X-8.8-0.5 M-673 K, (c) CoO_x-X-8.8-1 M-673 K, (d) CoO_x-X-8.8-5 M-673 K, (e) CoO_x-X-8.8-0.1 M-573 K, (f) CoO_x-X-8.8-0.1 M-923 K, and (g) Co_3O_4.

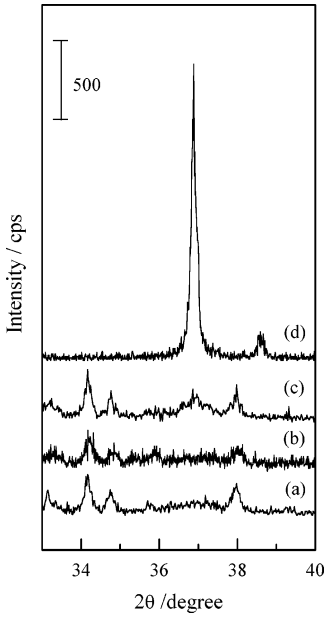

Figure 3. XRD patterns of the CoO_x-Y samples with the cobalt content of 6.2 wt % obtained by changing the calcination temperature, as well as Co_3O_4: (a) CoO_x-Y-6.2-0.1 M-573 K, (b) CoO_x-Y-6.2-0.1 M-673 K, (c) CoO_x-Y-6.2-0.1 M-923 K, and (d) Co_3O_4.

appeared as the strongest diffraction peak of Co_3O_4, could be discerned (curve d in Figure 2), while only diffraction peaks of NaY were observed with lower concentrations of NaOH. Calculations using the Scherrer equation revealed that the size of the Co_3O_4 particles was ca. 9 nm in the case of using 5.0 M NaOH. For the effect of the calcination temperature, it can be seen from Figure 2 that no peak ascribed to crystalline Co_3O_4 appears at calcination temperatures of 573 and 673 K (curves e and a), whereas a peak at 36.8° is clearly observed as the calcination temperature is raised to 923 K (curve f). The Co_3O_4 particles were evaluated to be ca. 29 nm in size by the Scherrer equation. The results described above suggest that the use of a high concentration of NaOH in the precipitation step and high calcination temperature both result in relatively large Co_3O_4 particles (9−29 nm), and the effect of calcination temperature is more notable. Similar results have been obtained for the CoO_x-Y samples, and the effect of calcination temperature is shown in Figure 3. These relatively large Co_3O_4 particles must be located outside the supercages of X or Y zeolite. It is expected that the diffusion of CoO_x particles would become easier at higher temperatures, and thus, the CoO_x particles may have higher probability to migrate out of the supercages and aggregate to form large and stable Co_3O_4 particles.

N_2-Sorption Results. N_2 adsorption−desorption isotherms of NaX, NaOH-treated NaX, and CoO_x-containing X zeolites are shown in Figure 4. The isotherms of NaX showed a shape (type I) characteristic of microporous materials. After the treatment with 0.1 M NaOH, a small hysteresis loop was observable, and this loop became considerable for the CoO_x-X (Co, 8.8 wt %) sample calcined at 673 K. This observation indicates

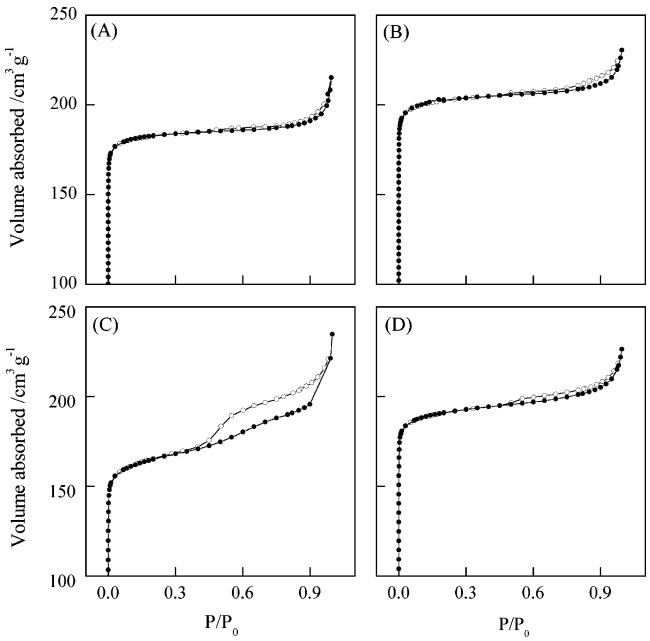

Figure 4. N_2 adsorption−desorption isotherms of NaX, NaOH-treated NaX, and CoO_x-containing X zeolites: (A) NaX, (B) NaX-0.1 M NaOH, (C) CoO_x-X-8.8-0.1 M-673 K, and (D) CoO_x-X-8.8-0.1 M-923 K.

that mesopores are generated in these two samples. Figure 5 shows the pore size distributions for these samples evaluated by the HK method in the microporous region (0.5−1.5 nm, Figure 5A) and the BJH method in the mesoporous region (2−50 nm, Figure 5B). The size of the micropores was estimated to be 0.81 nm for NaX and became larger after the treatment with NaOH. It was further enlarged to 0.98 nm for the CoO_x-X sample calcined at 673 K. The formation of mesopores with size of ca. 3.8 nm was most notable for this sample (Figure 5B). The formation of mesopores was also observed by Wark and co-workers when NaX

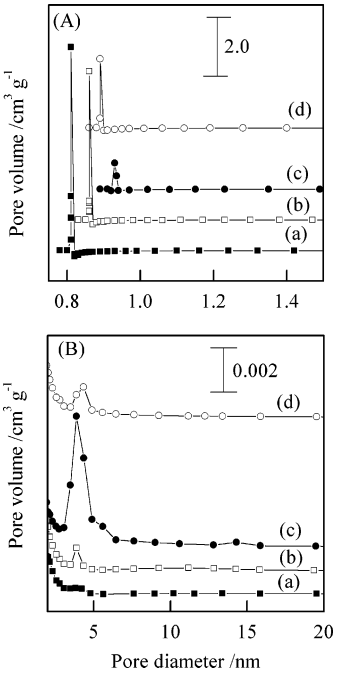

Figure 5. Pore size distributions evaluated by the HK method in the microporous region (A) and the BJH method in the mesoporous region (B): (a) NaX, (b) NaX-0.1 M NaOH, (c) CoO_x-X-8.8-0.1 M-673 K, and (d) CoO_x-X-8.8-0.1 M-923 K.

Table 2. Parameters of Porous Structures Determined by N_2 Sorption

sample	BET surf. area (m^2 g^{-1})	mean pore diameter (nm)	$V_{<1.5}$[c] (cm^3 g^{-1})	$V_{1.5-5}$ (cm^3 g^{-1})	V_{5-50}[c] (cm^3 g^{-1})
NaX	608	0.83	0.263	0.012	0.023
NaX-0.1 M NaOH[a]	671	0.86	0.277	0.014	0.025
Co^{2+}-X-8.8[b]	647	0.92	0.271	0.035	0.027
CoO_x-X-8.8-673 K	553	1.00	0.217	0.071	0.047
CoO_x-X-8.8-923 K	637	0.90	0.268	0.024	0.018
NaY	686	0.88	0.376	nd[d]	nd
CoO_x-Y-6.2-673 K	564	1.17	0.261	nd	nd

[a] NaX zeolite was treated with 0.1 M NaOH followed by calcination at 673 K. [b] The Co^{2+}-exchanged sample followed directly by calcination at 673 K without precipitation step. [c] $V_{<1.5}$, $V_{1.5-5}$, and V_{5-50} denote volumes of pores with diameters <1.5, 1.5−5, and 5−50 nm, respectively. [d] Not detected.

or NaY zeolite was treated with NaOH.[8] As speculated by Wark and co-workers,[8] although the dealuminization of the zeolite might cause mesopores, the removal of a small part of the silicon atoms in the framework by the attack of hydroxyl ions should mainly be responsible for the formation of mesopores with sizes even larger than 2 nm. This process may be accelerated by the presence of Co^{2+}, possibly because the energy released during the exothermic precipitation of $Co(OH)_2$ contributed to the splitting of the Si−O bonds in the framework. This may explain why the CoO_x-X sample (Figures 4C and 5B) shows a remarkably larger proportion of mesopores than the NaOH-treated NaX sample without cobalt.

The parameters of the porous structures calculated on the basis of the N_2 adsorption−desorption isotherms are summarized in Table 2. The treatment of NaX zeolite with NaOH slightly increased the surface area and the volumes of both micropores and mesopores. The formation of CoO_x by precipitating Co^{2+} with NaOH in the supercages of NaX zeolite followed by calcination at 673 K remarkably decreased the volume of micropores. This was also observed in the case of forming

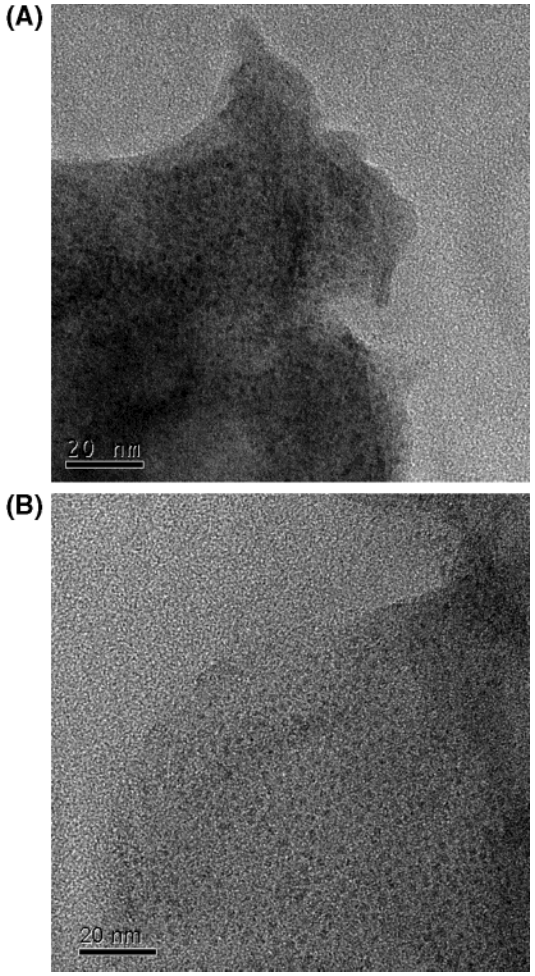

Figure 6. TEM micrographs of the CoO_x-X and CoO_x-Y samples prepared under the standard conditions: (A) CoO_x-X-8.8-0.1 M-673 K and (B) CoO_x-Y-6.2-0.1 M-673 K.

CoO_x in NaY zeolite. However, as the CoO_x-X sample was calcined at 923 K, the surface area and volume of micropores were restored again. We speculate that this may be related to the migration of CoO_x out of the pores of zeolites after the calcination at 923 K.

TEM Results. The TEM micrographs of the CoO_x-X sample with cobalt content of 8.8 wt % and the CoO_x-Y sample with cobalt content of 6.2 wt % prepared under the standard conditions are shown in Figure 6. We can discern a homogeneous distribution of small CoO_x particles inside the zeolites in both cases. The particles were mostly observed in the size range of 0.7−3 nm with a maximum of size distribution at 1.3−1.5 nm in both cases (Figure 7). Particles larger than 3 nm were hardly seen in these two samples. EDS measurements reveal homogeneous distributions of cobalt in both samples and typical spectra in both cases are shown in Figure 8. The strong signals of Cu in Figure 8 were due to the Cu grid used for the TEM observations. Considering the size (1.3 nm) of supercage of faujasite zeolites and the formation of a small portion of mesopores after the precipitation of Co^{2+} with diluted NaOH (Figures 4 and 5 and Table 2), it is reasonable to conclude that most of the CoO_x particles are located inside the supercages and the generated mesopores of zeolites.

Figure 9 shows the TEM micrograph of the CoO_x-X sample with the same cobalt content of 8.8 wt % but calcined at 923 K. Relatively large cobalt oxide particles

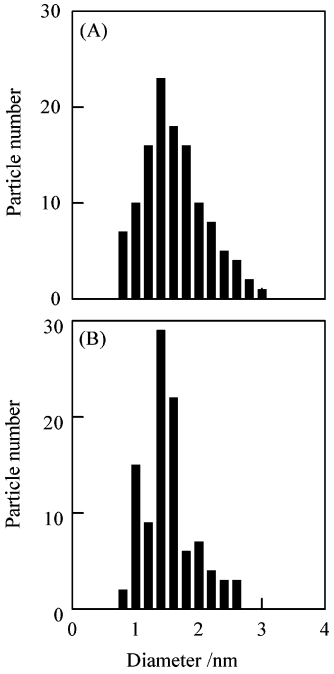

Figure 7. (A) CoO_x particle size distribution in CoO_x-X-8.8-0.1 M-673 K and (B) CoO_x particle size distribution in CoO_x-Y-6.2-0.1 M-673 K.

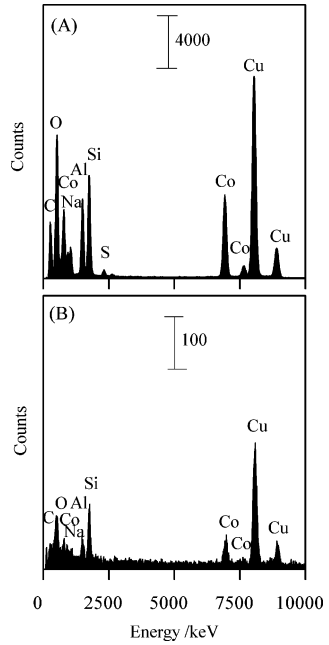

Figure 8. EDS spectra of the CoO_x-X and CoO_x-Y samples prepared under the standard conditions: (A) CoO_x-X-8.8-0.1 M-673 K and (B) CoO_x-Y-6.2-0.1 M-673 K.

with sizes of ca. 20 nm could be observed in this material. EDS analyses in Figure 10 clearly show that the distributions of cobalt in this material are not homogeneous. For the analysis area without large cobalt oxide particles (Figure 10A), the relative strength of the cobalt signal in the EDS spectrum was lower as compared with the sample calcined at 673 K (Figure 8A). On the other hand, if the analysis was focused on the large particles (Figure 10B), almost only cobalt and oxygen were observed in addition to copper and carbon arising from the support grid, and the relative intensities of the silicon and aluminum peaks were very weak. This confirms the presence of large CoO_x particles in this sample. The observations described here are consistent with the XRD result shown in Figure 2, indicating that the small CoO_x particles migrate outside the supercage to form larger Co_3O_4 particles when a high calcination temperature is applied.

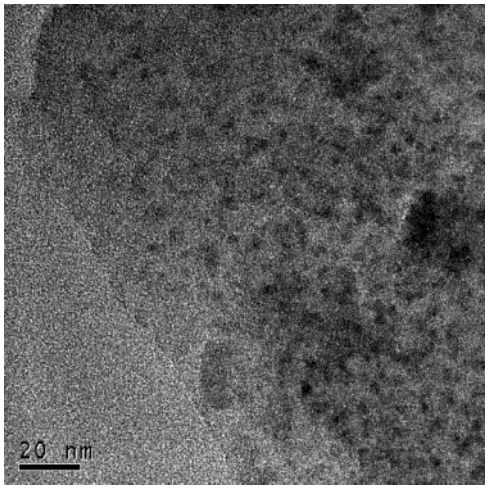

Figure 9. TEM micrograph of the CoO_x-X sample with cobalt content of 8.8 wt % calcined at 923 K.

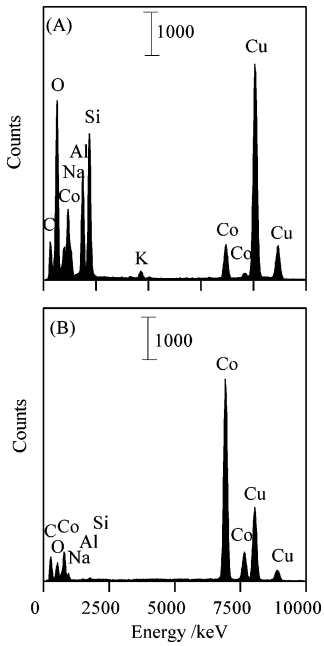

Figure 10. EDS spectra of the CoO_x-X sample with cobalt content of 8.8 wt % calcined at 923 K. (A) The analysis area without large CoO_x particles and (B) the analysis on the large CoO_x particles.

XPS Results. XPS is a surface-sensitive technique, and the sampling depth is less than 3 nm in general. However, because of the large voids of the faujasite zeolite, the effective information for Co 2p has been estimated to be capable of reaching ca. 14 nm in depth, corresponding to ca. five unit cells of the zeolite below the surface.[33] Therefore, the information from XPS can be used to discuss the oxidation state of cobalt of the CoO_x particles within the supercages.

Figure 11 shows the Co 2p XPS spectra for the CoO_x-X samples prepared under different conditions as well as

(33) Guczi, L.; Bazin, D. *Appl. Catal. A* **1999**, *188*, 163.

Table 3. Deconvolution Results for Co $2p^{3/2}$ [a]

	ionic Co(II)			oxidic Co(II)			oxidic Co(III)				
sample	BE (eV)	fwhm (eV)	peak area	BE (eV)	fwhm (eV)	peak area	BE (eV)	fwhm (eV)	peak area	oxidic Co(II)/ oxidic Co(III)	CoO/ Co_3O_4[b]
Co_3O_4	–	–	–	780.4	2.43	8003	779.4	2.00	16037	0.50	0
Co^{2+}-X-8.8-673 K[c]	781.7	3.05		–	–	–	–	–	–	–	–
CoO_x-X-8.8-0.1 M-673 K	781.7	2.79	4143	780.4	2.40	4505	779.4	2.00	1237	3.64	3.14
CoO_x-X-8.8-0.1 M-923 K	781.7	2.81	3645	780.4	2.41	3472	779.4	2.10	4596	0.76	0.31
CoO_x-X-8.8-5 M-673 K	781.7	2.83	3205	780.4	2.39	6439	779.4	2.01	4529	1.42	0.92
CoO_x-Y-3.5-0.1 M-673 K	781.7	2.76	1270	780.4	2.42	2710	779.4	2.02	601	4.51	4.01
CoO_x-Y-6.2-0.1 M-673 K	781.7	2.73	1727	780.4	2.43	4107	779.4	1.96	1121	3.66	3.16
CoO_x-Y-6.2-0.1 M-923 K	781.7	2.79	809	780.4	2.37	3665	779.4	2.10	3806	0.96	0.46

[a] BE and fwhm denote binding energy and full width at half-maximum, respectively. [b] This was calculated by assuming that the oxidic Co(III) is contained in Co_3O_4 and the oxidic Co(II) is contained in both Co_3O_4 and CoO. [c] This sample was prepared by directly calcining the exchanged zeolite without the precipitation step.

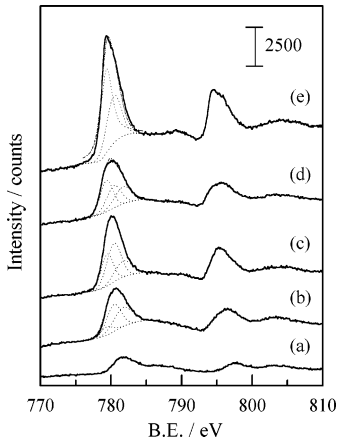

Figure 11. Co 2p XPS spectra for the CoO_x-X samples prepared under different conditions, as well as the Co^{2+}-X sample and Co_3O_4: (a) Co^{2+}-X, (b) CoO_x-X-8.8-0.1 M-673 K, (c) CoO_x-X-8.8-5 M-673 K, (d) CoO_x-X-8.8-0.1 M-923 K, (e) Co_3O_4.

the Co^{2+}-X sample and Co_3O_4 as references. The binding energy of Co $2p^{3/2}$ for the Co^{2+}-X sample prepared by directly calcining the Co^{2+}-exchanged X zeolite is 781.7 eV, which can be attributed to the Co^{2+} ion exchanged in the zeolite.[33] Therefore, the cobalt species in the sample without the precipitation step remained mainly as Co^{2+} even after calcination at 673 K. For the samples after the precipitation step, the binding energy of Co $2p^{3/2}$ remarkably shifted to lower values. Furthermore, the concentration of NaOH used for precipitation and the calcination temperature also affected the values of binding energy of Co $2p^{3/2}$. The sample with 5 M NaOH for precipitation of Co^{2+} in the preparation and that calcined at 923 K exhibited lower values of binding energy as compared with that prepared under the standard conditions, and the values approached that for Co_3O_4. These results strongly suggest that the oxidation states of cobalt in these samples are different.

Referenced to the binding energies of Co $2p^{3/2}$ in different compounds,[34] the peak of Co $2p^{3/2}$ was deconvoluted into three components, i.e., Co(II) in the ionic state (at an exchange site) at 781.7 eV, Co(II) in an oxide state at 780.4 eV, and Co(III) in an oxide state at 779.4 eV (Figure 11). The peak of Co $2p^{3/2}$ for Co_3O_4 could be deconvoluted to oxidic Co(III) and Co(II) without ionic Co(II), and the ratio of the areas of the two peaks was calculated to be 2.0, in good agreement with the fact that Co_3O_4 comprises oxidic Co(III) and Co(II) with a ratio of 2:1. The CoO_x-X samples prepared under different conditions contained the three components, i.e., ionic Co(II) and oxidic Co(II) and Co(III), but the ratios of the three components were different. Similar results were likewise observed for the CoO_x-Y samples.

The detailed deconvolution results are summarized in Table 3. It is interesting to note that the CoO_x-X sample prepared under the standard conditions exhibits a remarkably higher ratio of oxidic Co(II) to oxidic Co(III) than Co_3O_4. This indicates that most CoO_x species in this sample exist in the state of CoO, and only a small part exists in the state of Co_3O_4. By assuming that all the oxidic Co(III) and a part of oxidic Co(II) are contained in Co_3O_4, the ratio of CoO to Co_3O_4 has been calculated to be 3.14 for this sample. This ratio decreased drastically to 0.31 and 0.92 when the calcination temperature of 923 K and the concentration of NaOH of 5 M were applied to prepare the CoO_x-X samples, respectively, showing that a large proportion of Co_3O_4 was formed by using these preparation conditions. Very similar results have likewise been obtained for the CoO_x-Y samples (Table 2). These observations, combined with the XRD and TEM results, strongly suggest that the CoO_x species inside the supercages of zeolite exist mostly in the state of $Co^{II}O$, while they are changed into Co_3O_4 after migrating outside the supercages.

The results in Table 2 also reveal that the ionic Co(II) species still remain in large quantity even with the precipitation step. A large number of studies have contributed to the elucidation of the cation distribution in faujasite zeolites, and it has been clarified that cations can occupy several different types of sites with different locations and potential energies, i.e., sites I, I′, II, II′, III, and III′ (Figure 12).[35,36] Sites III, III′, and II are located inside the supercages, while the other sites are inside the sodalite cages and the hexagonal prisms. With the sizes mostly in 0.8−3 nm, the encapsulated CoO_x particles must be located inside the supercages and the mesopores generated during the preparation step. Furthermore, it is reasonable to consider that the precipitation mainly occurs within the supercage, since the smaller windows to the hexagonal prisms and the sodalite cages would hinder the access of sodium

(34) Moulder, J. F.; Stickle, W. F.; Sobol, P. E.; Bomben, K. D. *Handbook of X-ray Photoelectron Spectroscopy*; Chastain, J., King, R. C., Jr., Ed.; Physical Electronics, Inc.: Minnesota, 1995.

(35) Buttefey, S.; Boutin, A.; Mellot-Draznieks, C.; Fuchs, A. H. *J. Phys. Chem. B* **2001**, *105*, 9569.

(36) (a) Bae, D.; Seff, K. *Microporous Mesoporous Mater.* **1999**, *33*, 265. (b) Lee, S. H.; Kim, Y.; Seff, K. *J. Phys. Chem. B* **2000**, *104*, 2490.

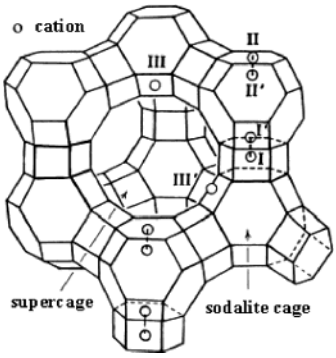

Figure 12. Schematic view of a faujasite supercage and cation locations.

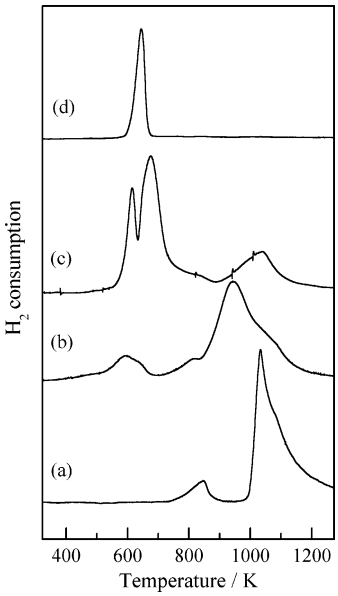

Figure 13. TPR profiles of the CoO_x-containing NaX zeolites, as well as the Co^{2+}-X sample and Co_3O_4: (a) Co^{2+}-X, (b) CoO_x-X-8.8-0.1 M-673 K, (c) CoO_x-X-8.8-0.1 M-923 K, and (d) Co_3O_4.

hydroxide in addition to the limit in their spaces. Moreover, the cations in these locations possess stronger interactions with the zeolite framework. Therefore, we conclude that the remaining Co^{2+} ions are within the sodalite cages and possibly the hexagonal prisms. It should be noted that the proportion of these remaining Co^{2+} ions decreased when the CoO_x-X or the CoO_x-Y sample was calcined at 923 K. This is different from the phenomenon observed for the ion-exchanged faujasite zeolites, where the increase in calcination temperature would result in the migration of cations into the sodalite cages and hexagonal prisms.[2]

H_2-TPR Results. The reduction behaviors of the CoO_x-X and CoO_x-Y materials have been investigated by H_2-TPR. Figure 13 shows the results obtained for the CoO_x-X samples prepared under different conditions, as well as the Co^{2+}-X sample and Co_3O_4 as references. For the crystalline Co_3O_4, only one sharp reduction peak was observed at 644 K. On the other hand, the reduction of Co^{2+} in the Co^{2+}-X sample took place at temperatures higher than 773 K with the main reduction peak at 1023 K. A small reduction occurring with a peak at 823 K was also observed. The reduction peaks observed at 823 and 1023 K for the Co^{2+}-X sample probably corresponded to the reduction of Co^{2+} ions exchanged at different sites of NaX zeolite with different potential

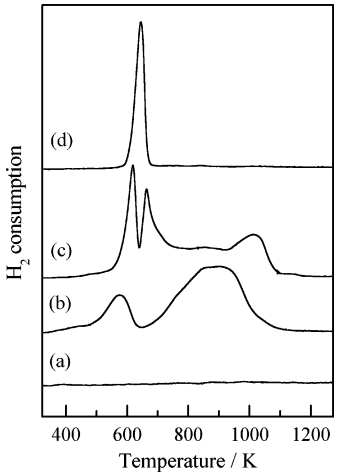

Figure 14. TPR profiles of the CoO_x-containing NaY zeolites, as well as the Co^{2+}-Y sample and Co_3O_4: (a) Co^{2+}-Y, (b) CoO_x-Y-6.2-0.1 M-673 K, (c) CoO_x-Y-6.2-0.1 M-923 K, and (d) Co_3O_4.

energy. For the CoO_x-X sample prepared under the standard conditions, the reduction began to occur at temperatures lower than 573 K and was characterized by very broad peaks in two temperature regions, i.e., 473−650 and 673−1100 K. The broad feature was probably related to the reduction of cobalt species inside the pores of the zeolite. In general, relatively sharp reduction peaks at ca. 593−673 K were observed for CoO, Co_3O_4, and the supported cobalt oxides.[37−39] We thus suggest that the broad peak at 473−650 K is caused by the reduction of the cobalt oxide particles, most of which are in the state of CoO, in the supercages of zeolite X. On the other hand, the broad peak at 673−1073 K is tentatively ascribed to the reduction of the remaining Co^{2+} and possible some CoO_x clusters with strong interaction with the framework, since the ions that have interacted with the zeolite framework are more difficult to reduce as compared with cobalt oxides. As compared with the Co^{2+}-X sample, the reduction of the Co^{2+} ions in the CoO_x-X sample finished at a lower temperature and the peak temperature also shifted to a lower temperature. For a few zeolite-supported bimetallic systems such as Pd−Ni/NaY, the reducibility of the nickel ions in zeolite cages was found to be enhanced by the presence of metallic Pd near by.[40] We thus speculate that the metallic cobalt produced by the reduction of the encapsulated CoO at lower temperatures may enhance the reduction of Co^{2+} remaining in the zeolite cages.

The CoO_x-Y sample prepared under the standard conditions exhibited very similar H_2-TPR profiles (Figure 14) to the CoO_x-X sample, and accordingly, the peak at 473−650 K was assigned to the reduction of CoO_x (mainly CoO) encapsulated in zeolite Y, while the peak at 673−1073 K was ascribed to the reduction of Co^{2+} remaining in the zeolite cage and possibly a part of CoO_x having a strong interaction with the framework of zeolite Y. On the other hand, the Co^{2+}-Y did not show

(37) Arnoldy, P.; Moulijn, J. A. *J. Catal.* **1985**, *93*, 38.
(38) Boot, L. A.; Kerkhoffs, M. H. J. V.; van Dillen, A. J.; Geus, J. W.; van Buren, F. R.; van der Linden, B. Th. *Appl. Catal. A* **1996**, *137*, 69.
(39) Sun, S.; Tsubaki, N.; Fujimoto, K. *Appl. Catal. A* **2000**, *202*, 121.
(40) Guczi, L.; Kiricsi, I. *Appl. Catal. A* **1999**, *186*, 375.

any peaks during the TPR measurement up to 1200 K. As compared with the Co^{2+}-X sample, the lower reducibility of the Co^{2+}-Y probably arises from the relatively higher Si/Al ratio and the lower cobalt content in this sample. These make the Co^{2+} ions in this sample occupy sites I, I′, II, and II′ only, while Co^{2+} in the Co^{2+}-X sample may occupy sites III and III′ (Figure 12), which are believed to be of higher potential energy and can be reduced at lower temperatures. The enhancement of the reduction of the remaining Co^{2+} in the CoO_x-Y was much more notable.

For the CoO_x-X and CoO_x-Y samples calcined at 923 K, the TPR profiles changed significantly. Two sharper peaks appeared in the temperature range of 573−673 K. The peak area of the broad peak at 873−1073 K became remarkably small, and the position of this high-temperature peak shifted to a higher temperature. We speculate that this may relate to the migration of a part of the CoO_x out of the supercages of the zeolites and the formation of larger Co_3O_4 particles, as suggested by the XRD, TEM, and XPS results described above. It seems likely that the peak at ca. 664 K results from the reduction of the Co_3O_4 particles outside the supercages of the zeolite while that at ca. 613 K results from that of the CoO particles occluded inside the supercages. However, the supported small Co_3O_4 particles may also exhibit two H_2-TPR peaks at 593−673 K, which are generally believed to correspond to the stepwise reduction of Co_3O_4 to CoO and of CoO to Co.[38,39] Therefore, we speculate that these two peaks may comprise both the stepwise reduction of Co_3O_4 and the reduction of the remaining CoO without migration out of the supercage. The smaller proportion of the broad TPR peak at 873−1073 K after calcination at 923 K indicates that a lower amount of Co^{2+} ions remained in the zeolites. This is essentially consistent with the XPS results.

The H_2-TPR profiles obtained here have been compared with those reported for Co/ZSM-5. For the Co/ZSM-5 prepared by a couple of methods such as impregnation and sublimation, TPR peaks at 968−978 K for Co^{2+} ions, at 658−663 K for Co_3O_4, and in a low-temperature region (493−523 K) were observed.[41,42] The peak in the low-temperature region was proposed to arise from the reduction of Co^{II} oxo ions or Co^{II} oxo clusters within the ZSM-5. This peak may relate to the low-temperature peak (473−650 K) observed in our case. According to our analyses as described above, we ascribed the low-temperature peak in our case to the reduction of $Co^{II}O$ within the faujasite zeolites.

The rationality of our assignments described above was further checked by quantitative calculations. For the samples calcined at 923 K (curve c in Figures 13 and 14), the total consumption of H_2 in H_2-TPR roughly corresponded to the reduction of Co_3O_4 to Co, i.e., ca. 1.3 mol (roughly 4/3 mol) of H_2 consumed per mol of Co. However, only ca. 0.9 mol of H_2 was consumed per mole of Co for the samples calcined at 673 K (curve b in Figures 13 and 14). These calculations support the conclusion that Co_3O_4 particles mainly exist in the samples calcined at 923 K, while CoO or Co^{2+} exists in those calcined at 673 K. On the basis of the assumption that the states of cobalt oxide particles were CoO and Co_3O_4 in the samples calcined at 673 and 923 K, respectively, and the reduction peaks before 673 K corresponded to the transformation of these oxides to Co, we quantitatively calculated the reduction degrees at 673 K for the CoO_x-X and the CoO_x-Y samples. It has been confirmed that the reduction at 673 K can keep the metallic cobalt particles within the supercages of zeolites while higher reduction temperature would lead to the migration of metallic cobalt out of the zeolite cages. The results shown in Table 4 revealed that the reduction degree at 673 K for the CoO_x-X and CoO_x-Y samples calcined at 673 K, in which CoO_x particles existing mainly as CoO were encapsulated within the supercages of zeolites, were 15−17% and 21−26%, respectively. The same samples calcined at 923 K exhibited remarkably higher reduction degrees. The results obtained from O_2 titration for several samples reduced at 673 K resembled essentially those calculated from TPR experiments.

Table 4. Reduction Degrees at 673 K for the CoO_x-X and CoO_x-Y Samples

sample	reduction degree (%)	
	calcd from TPR	measured by O_2-titration
CoO_x-X-5.7-673 K	17	15
CoO_x-X-8.8-673 K	16	15
CoO_x-X-8.8-923 K	74	75
CoO_x-Y-3.5-673 K	23	nd[a]
CoO_x-Y-6.2-673 K	21	27
CoO_x-Y-6.2-923 K	74	nd

[a] Not detected.

Table 5. Catalytic Results of the CoO_x-X and the CoO_x-Y Samples Reduced at 673 K for Fischer−Tropsch Synthesis[a]

sample	CO convn (%)	selectivity (%)		α
		CH_4	C_5^+	
CoO_x-X-2.6-673 K	10.4	10.7	80.5	0.85
CoO_x-X-5.7-673 K	45.3	12.4	82.7	0.81
CoO_x-X-8.8-673 K	65.9	11.1	85.4	0.82
CoO_x-X-9.5-673 K	80.9	15.1	79.7	0.80
CoO_x-X-8.8-923 K	30.7	10.4	82.8	0.86
CoO_x-Y-2.5-673 K	37.5	15.2	78.2	0.77
CoO_x-Y-3.5-673 K	64.5	11.6	82.7	0.80
CoO_x-Y-6.2-673 K	77.2	17.1	75.0	0.76
CoO_x-Y-6.2-923 K	59.4	8.4	88.2	0.86

[a] Reaction conditions: sample weight, 0.8 g; $H_2/CO = 2$; pressure, 2.0 MPa; flow rate, 20 $cm^3\ min^{-1}$.

Catalytic Results. The CoO_x-X and the CoO_x-Y samples after reduction at 673 K have been applied to Fischer−Tropsch synthesis, and the results are shown in Table 5. It should be noted here that, after reduction with H_2 at 673 K, the Co^{2+}-X (Co, 8.7 wt %) and Co^{2+}-Y (Co, 6.2 wt %) samples, which were prepared by directly calcining the Co^{2+}-exchanged zeolites (without precipitation step), did not show any CO conversions in Fischer−Tropsch synthesis. This is because the Co^{2+} ions exchanged in faujasite zeolites cannot be reduced at 673 K (Figures 13 and 14). On the other hand, the CoO_x-X and CoO_x-Y samples reduced at 673 K exhibited considerable CO conversions, as shown in Table 5. The activity was stable over these samples, and the CO conversion shown here was obtained after 10 h of reaction. The product distributions were similar over

(41) Wang, X.; Chen, H.-Y.; Sachtler, W. M. H. *Appl. Catal. B* **2000**, *26*, L227.
(42) Schwartz, V.; Prins, R.; Wang, X.; Sachtler, W. M. H. *J. Phys. Chem. B* **2002**, *106*, 7210.

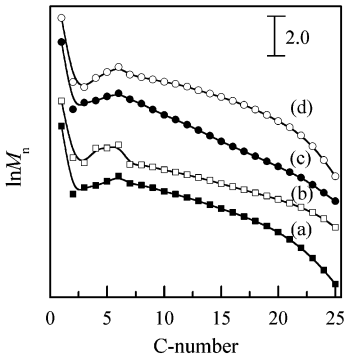

Figure 15. Anderson−Schulz−Flory distributions: (a) CoO_x-X-8.8-673 K, (b) CoO_x-X-8.8-923 K, (c) CoO_x-Y-6.2-673 K, and (d) CoO_x-Y-6.2-923 K.

these samples. The selectivity to C_5^+ hydrocarbons reached or exceeded 80%. The Anderson−Schulz−Flory (ASF) distributions for the reduced CoO_x-X samples with a cobalt content of 8.8 wt % and the reduced CoO_x-Y samples with a cobalt content of 6.2 wt % calcined at both 673 and 923 K are summarized in Figure 15. The distributions shown in Figure 15 all deviated from the ideal ASF distribution with a deficiency in C_2-C_5 hydrocarbons. This phenomenon was also observed over other cobalt catalysts supported on porous silica.[43] Values of the chain growth probability (α) calculated from these curves were in the range of 0.76−0.86 (Table 5).

It is interesting to note that, as compared with the samples calcined at 673 K, the samples with the same cobalt content but calcined at 923 K exhibited remarkably lower CO conversions, although the latter samples possessed higher reduction degrees, as shown in Table 4. This result strongly suggests that the smaller cobalt particles encapsulated within the supercages of faujasite zeolites are more active than the larger ones located outside the supercages.

(43) Ernst, B.; Libs, S.; Chaumette, P.; Kiennemann, A. *Appl. Catal. A* **1999**, *186*, 145.

Conclusions

The cobalt oxide particles within faujasite zeolites synthesized by a procedure comprising (i) ion-exchange of cobalt ions into zeolites, (ii) precipitation of cobalt ions with sodium hydroxide inside the pores of zeolites, and (iii) calcination have been characterized in detail. These cobalt oxide particles are in the size range of 0.7−3 nm with a maximum of size distribution at 1.3−1.5 nm and are mainly in the state of $Co^{II}O$. The concentration of sodium hydroxide for precipitation and the calcination temperature are crucial in controlling the location and state of the cobalt oxide. A higher concentration of sodium hydroxide and higher calcination temperature will lead to large cobalt oxide particles (ca. 20 nm) in the state of Co_3O_4, which are located outside the zeolite pores. The cobalt oxide particles encapsulated inside the supercage can be partly reduced at temperatures as low as 573 K, and the reduction is characterized by a very broad peak. The metallic cobalt formed by the reduction of the encapsulated nanosized cobalt oxide exhibits higher CO conversion in Fischer−Tropsch synthesis.

Acknowledgment. This work was supported by the Natural Science Foundation of China (Nos. 20021002 and 20373055), the Chinese Ministry of Science and Technology (No. G1999022408), and the National Basic Research Program of China (No. 2003CB615803).

CM030626Z